Journal of Atmospheric and Solar–Terrestrial Physics 218 (2021) 105596

Contents lists available at ScienceDirect

Journal of Atmospheric and Solar-Terrestrial Physics

journal homepage: www.elsevier.com/locate/jastp

Sounding rocket project "PMWE" for investigation of polar mesosphere winter echoes☆

Boris Strelnikov [a,*], Tristan Staszak [a], Ralph Latteck [a], Toralf Renkwitz [a], Irina Strelnikova [a], Franz-Josef Lübken [a], Gerd Baumgarten [a], Jens Fiedler [a], Jorge L. Chau [a], Joan Stude [c,b], Markus Rapp [b,c], Martin Friedrich [d], Jörg Gumbel [e], Jonas Hedin [e], Evgenia Belova [h], Marcus Hörschgen-Eggers [f], Gabriel Giono [a,g], Igor Hörner [i], Stefan Löhle [i], Martin Eberhart [i], Stefanos Fasoulas [i]

[a] Leibniz-Institute of Atmospheric Physics at the Rostock University (IAP), Kühlungsborn, Germany
[b] Deutsches Zentrum für Luft- und Raumfahrt, Institut für Physik der Atmosphäre (IPA), Oberpfaffenhofen, Germany
[c] Ludwig-Maximilians-Universität München (LMU), Atmospheric Physics, München, Germany
[d] Graz University of Technology (TUG), Graz, Austria
[e] Department of Meteorology (MISU), Stockholm University, Stockholm, Sweden
[h] Swedish Institute of Space Physics (IRF), Kiruna, Sweden
[f] Deutsches Zentrum für Luft- und Raumfahrt, DLR MORABA, Oberpfaffenhofen, Germany
[g] Royal Institute of Technology (KTH), Stockholm, Sweden
[i] University of Stuttgart, Institute of Space Systems (IRS), Stuttgart, Germany

ARTICLE INFO

Keywords:
PMWE
Sounding rockets
In situ measurements
Radar echoes

ABSTRACT

A first sounding rocket campaign dedicated to investigate the creation mechanism of Polar Mesosphere Winter Echoes (PMWE) was conducted in April 2018 from the north Norwegian Andøya Space Center (69 ◦N, 16 ◦E). Two instrumented sounding rockets were launched on 13th and 18th of April under PMWE and non-PMWE conditions, respectively. In this paper we give an overview of the PMWE sounding rocket mission. We describe and discuss some results of combined in situ and ground-based measurements which allow to verify existing PMWE theories. Our measurements ultimately show that: a) polar winter mesosphere is abounded with meteor smoke particles (MSP) and intermittent turbulent layers, b) all PMWE observed during this campaign can be explained by neutral air turbulence, c) turbulence creates small-scale structures in all D-region constituents, including free electrons; d) MSP ultimately influence the radar volume reflectivity by distorting the turbulence spectrum of electrons, e) the influence of MSP and of background electron density is just to increase SNR.

1. Introduction

First observations of radar echoes in the very high frequency (VHF) range from polar mesosphere/lower thermosphere (MLT) region were reported about forty years ago by Czechowsky et al. (1979) and Ecklund and Balsley (1981). The echoes were observed at high northern latitudes almost all over the year. Already Ecklund and Balsley (1981) noted profound distinction between these echoes during winter and summer seasons. In winter these echoes were significantly weaker and came from much lower altitudes, 55–85 km, whereas in summer the radar returns were from approx. 75 to 100 km. Subsequent observations showed that these radar echoes are much more frequent in summer, whereas in

☆ Supported by:
Supported by:
Federal Ministry for Economic Affairs and Energy
on the basis of a decision by the German Bundestag

* Corresponding author.
E-mail address: strelnikov@iap-kborn.de (B. Strelnikov).

https://doi.org/10.1016/j.jastp.2021.105596
Received 30 November 2020; Received in revised form 17 February 2021; Accepted 23 February 2021
Available online 29 March 2021

winter they are rather rare.

Huge scientific efforts were made to understand the nature of these echoes which led to conclusion that their formation mechanism in summer must be different from those in winter. Therefore, these echoes were named Polar Mesosphere Summer echoes, PMSE (after Röttger et al., 1988; Hoppe et al., 1988) and Polar Mesosphere Winter Echoes, PMWE (after Kirkwood et al., 2002). The high occurrence rate of PMSE made it possible to study them also in situ by using sounding rockets. Today it is commonly accepted that PMSE are caused by neutral air turbulence acting on charged ice particles ultimately forming coherent structures in electron density (see e.g., Cho and Kelley, 1993; Rapp and Lübken, 2004, and references therein). That is, the necessary condition for the formation of PMSE is the presence of ice particles in the mesosphere. This condition is well fulfilled at high latitudes in summer, whereas it is definitely not possible in winter because of much higher temperatures.

Due to the very low occurrence rate of PMWE, our understanding of them still remains ambiguous. To say exactly, there are several theories which can explain some of the observed echoes. These theories are mostly supported by indirect observations or by using typical values observed in this altitude region. In other words, there are no convincing direct confirmations of the PMWE theories.

The PMWE sounding rocket project aims at measuring in situ of atmospheric parameters which are most important to support (or reject) existing theories. In this paper we give a short overview of the existing theories of PMWE in Sec. 2, describe the sounding rocket project and payloads in Sec. 3, and give an overview of the 1st rocket campaign in Sec. 4. In Sec. 5 we briefly discuss the first results and give a summary in Sec. 6. A detailed analysis of in situ measurements conducted during the first rocket launch is given in the companion paper by Staszak et al. (2020).

2. Brief theory of coherent radar echoes

2.1. Coherent structures in mesosphere

Briefly explained, the coherent radar echoes at VHF (either PMSE or PMWE) are created by irregularities in the radio refractive index at the radar's Bragg scale (e.g., Gage, 1990; Hocking et al., 2016). The radar refractive index in the mesosphere is almost solely defined by the electron density (e.g., Gage, 1990; Hocking, 2003). That is, PMSE or PMWE are ultimately caused by coherent structures at the radar Bragg scale in the electron density.

Ottersten (1969) summarized formulae for coherent radar backscatter, where the radar volume reflectivity, or radar cross section per unit scattering volume is given by:

$$\eta(k) = \frac{\pi^2}{2} k^4 \varphi_n(k) \tag{1}$$

where k is the wave number of the probing radio wave, $\varphi_n(k)$ is three-dimensional (3D) spectrum of the refractive index of the scattering media. Woodman and Guillen (1974) derived a relation between the 3D spectra of the refractive index $\varphi_n(k)$ and of electron density fluctuations, $\varphi_{N_e}(k)$:

$$\varphi_n(k) = \frac{f_p^4}{4 f^4 N_e^2} \varphi_{N_e}(k) \tag{2}$$

where f_p is the plasma frequency, f is the frequency of the probing radio wave, N_e is the electron number density. Eqs. (1) and (2) together give an expression for radar volume reflectivity as a function of electron density fluctuations:

$$\eta(k) = \frac{\pi^2}{2} k^4 \frac{f_p^4}{4 f^4} \frac{\varphi_{N_e}(k)}{N_e^2} \tag{3}$$

Based on the formulae given by Ottersten (1969) and Woodman and Guillen (1974), Røyrvik and Smith (1984) derived an expression which relates the volume reflectivity with a one-dimensional (1D) spectrum of electron density fluctuation $S_{N_e}(k)$:

$$\eta(k) = p \frac{\pi}{8} k^2 \frac{f_p^4}{4 f^4} \frac{S_{N_e}(k)}{N_e^2} \tag{4}$$

where p is the power law of the spectral slope (e.g., $p = 5/3$ for inertial range turbulence) around the probing frequency f.

To summarize, the analytically derived Eq. (4) shows that the physical quantity η measured by radars is proportional to the 1D power spectrum $S_{N_e}(k)$ of electron density fluctuations measured in situ by a rocket instrument. Also, Røyrvik and Smith (1984) combined the terms $S_{N_e}(k)$ and N_e^2:

$$S_{\Delta N_e/N_e}(k) \equiv \frac{S_{N_e}(k)}{N_e^2} \tag{5}$$

and referred to it as a spectrum of relative variation in the electron density. This indeed follows from the linearity of the Fourier transform (cf. formulae by Woodman and Guillen, 1974).

To verify, whether the coherent radar echoes are created by turbulence, one has to measure the both η and either of $S_{N_e}(k)$ or $S_{\Delta N_e/N_e}(k)$ and check whether the proportionality given by Eq. (4) is satisfied inside PMSE/PMWE layers and not fulfilled outside the echoes. For radar echoes in summer, i.e. PMSE, this was repeatedly confirmed by rocket measurements (see e.g., Cho and Kelley, 1993; Kelley et al., 1987; Rapp and Lübken, 2004, and references therein). The difference between summer and winter echoes in this theory is the exact form of the spectrum $S_{N_e}(k)$ used in Eq. (4) (see below).

2.2. PMSE theory

Coherent structures responsible for PMSE can be created by neutral air turbulence. However, at altitudes of ~ 80 km and above (i.e. where PMSE are observed) turbulence acts at scales significantly larger than the MST radar Bragg scale (all the more so for the ISR). Thus, a radar frequency $f = 53$ MHz corresponds to the Bragg scale $\lambda_{Bragg} = 3$ m. The smallest turbulence scale known as Kolmogorov scale is given by $\eta_K = (\nu^3/\varepsilon)^{1/4}$, where ν is kinematic viscosity of air and ε is turbulence energy dissipation rate. Typical values for summer around 80 km yield $\nu = 1$ m^{2}s^{-1}, $\varepsilon = 10$ mWkg^{-1} (Lübken et al., 2002) and, therefore $\eta_K = 3.2$ m. That is, the smallest turbulent eddies exceed the Bragg scale and, therefore cannot directly explain radar echoes in summer. This problem is overcome when applying the theory of Batchelor (1959) to the charged constituents (see e.g., Cho et al., 1992; Lie-Svendsen et al., 2003; Rapp and Lübken, 2004; Rapp et al., 2008; Nicolls et al., 2009; Li et al., 2010; Varney et al., 2011). It is apparent that electron gas inside mesospheric ice clouds exhibits essentially reduced diffusivity, D_e, which can be expressed by the dimensionless Schmidt number as $Sc = \nu/D_e \gg 1$. Batchelor (1959)'s theory shows that such a scalar quantity (i.e. electron density fluctuations with $Sc \gg 1$) forms coherent structures at scales down to the so-called Batchelor scale $\lambda_B = \eta_K/\sqrt{Sc}$. This implies e.g., that for $Sc = 100$ the above shown estimate yields $\lambda_B = 0.3$ m for the electron densities. Note, that the observed Sc inside PMSE can easily reach values of several thousands (e.g., Strelnikov and Rapp, 2011). In other words, for the commonly observed values of ν and ε the electron gas reveals structuring at very small scales if its $Sc \gg 1$. This explains the PMSE and is convincingly confirmed by numerous in situ measurements (e.g., Cho et al., 1992; Cho and Kelley, 1993; Rapp and Lübken, 2004).

The physics of such reduced diffusivity is briefly as follows. The cold summer mesopause conditions lead to ice clouds in this altitude region (e.g., Lübken, 1999; Rapp and Thomas, 2006), which are immersed in the ionospheric plasma and, therefore, part of it becomes charged (e.g., Kelley et al., 1987; Cho et al., 1992; Rapp and Lübken, 2003). The

motion (and therefore diffusivity) of electrons is strongly coupled to (diffusive properties of) other charged plasma-constituents, which are ions and heavy charged aerosols (ice particles) (e.g., Chen, 2016; Cho and Kelley, 1993). These ice particles can be as large as 100 nm (e.g., Baumgarten et al., 2008; Hervig et al., 2009) and thereby, their diffusion coefficient is much lower than those of the surrounding air and it defines the diffusion properties of the ambient plasma. For more detailed explanation of the PMSE theory and supporting observations the reader is referred to Rapp and Lübken (2004).

2.3. PMWE theories

There are generally two classes of PMWE theories. The first class is based on neutral air turbulence as the key mechanism that creates coherent structures (Collis et al., 1992; Lübken et al., 2006, 2007; Rapp et al., 2011a; Morris et al., 2011). This class contains two theoretical explanations of the PMWE, namely by pure turbulence and by dusty turbulence, that is turbulence that contains heavy dust particles as minor constituent. The latter are known to be of meteoric origin (Rosinski and Snow, 1961; Hughes, 1997; Janches et al., 2006; Mathews et al., 2008) and often referred to as meteor smoke particles (MSP). Charged MSP produce similar effect on the ionospheric plasma as do charged ice particles inside PMSE, though less pronounced, owing to smaller sizes.

The second class of PMWE theories aimed to explain at least some strong, quasi specular PMWE moving with high horizontal speeds exceeding 300 ms^{-1} and is based on different physical process, namely on viscosity or ion-acoustic waves generated in situ in the mesosphere, suggested by Hocking et al. (1991) and Kirkwood et al. (2006b), respectively (see also Hocking et al., 2016, and references therein) and recently revised by Belova et al. (2020).

2.3.1. Pure turbulent theory of PMWE

In winter 2005 a sounding rocket campaign ROMA/WINTER was conducted at the Andøya Rocket Range (69 ◦N). The MST ALOMAR wind radar (ALWIN, Latteck et al., 1999), supported in situ measurements and by chance it observed PMWE. The campaign did not aim to investigate PMWE and, therefore there were no dedicated instruments to measure relevant parameters. However, this campaign yielded the first unprecedented in situ measurements for PMWE research. Lübken et al. (2006) and Brattli et al. (2006) showed that the observed PMWE below $\sim$ 70 km can well be explained by neutral air turbulence alone if the background ionization is high enough. The physics of radar echoes in this case is similar to that described above for PMSE, with the difference, that $Sc \approx 1$. That is, no charged aerosols are needed for coherent structures to be created at the radar Bragg scale.

Thus, a simple estimate shows that at 70 km altitude the typical (mean) values of kinematic viscosity and turbulence energy dissipation rate, $\nu = 0.1\ m^2 s^{-1}$ and $\varepsilon = 1$ mWkg^{-1} (Lübken, 1997), yield Kolmogorov scale of $\eta = (\nu^3/\varepsilon)^{1/4} = 1$ m, that is considerably smaller than the VHF radar Bragg scale of 3 m. Further below or/and when turbulence is stronger such structuring is present at even much smaller scales.

The spectral function that describes the observations in this case, that is of electron density fluctuations $S_{N_e}(k)$, is exactly the function applied for neutral air density fluctuations, $S_{N_e}(k) = S_{N_n}(k)$. It describes the universal equilibrium range of turbulent spectra which only contain two subranges, the inertial-convective and viscous-diffusive subranges. And there is no need to apply the Batchelor (1959)'s theory to explain radar echoes.

2.3.2. Dusty turbulence theory of PMWE

As mentioned above, IS radars such as EISCAT also observe PMWE (e.g., Strelnikova and Rapp, 2013), although their wavelength is significantly shorter than those of the MST radars. The Bragg scale of e. g., the EISCAT VHF radar is 0.7 m. If taken into account the sensitivity threshold of this radar of $\eta = 10^{-18}$m^{-1}, than even strong turbulence cannot explain PMWE observations in the manner done in the previous section. If, however, we recall that the winter mesosphere is "contaminated" by MSP, than it is evident that the entire lower ionosphere forms the so-called dusty plasma (e.g., Cho and Kelley, 1993; Shukla, 2001; Shukla and Mamun, 2001; Fortov et al., 2004, 2005). Rocket measurements show that MSP number density in the lower ionosphere in winter can be as large as 10^9 m^{-1} (e.g., Baumann et al., 2013, and references therein). This means, that the charged MSP is an important charge carrier which affects the behavior of the E– and D-region plasma (e.g., Friedrich and Rapp, 2009; Rapp et al., 2012). This in turn, suggests that MSP should play a similar role in the formation of coherent radar echoes in winter as it is done by the ice particles in summer (i.e., PMSE) and described in Sec. 2.2.

Quantitatively, the dusty turbulence theory of PMWE is essentially the same as the theory of PMSE. The only difference is that the charged aerosols are the MSP of the sizes of order of ~ 1 nm (e.g., Robertson et al., 2014; Asmus et al., 2017). Such relatively small heavy charged constituents produce comparably low Schmidt number of $Sc \sim 4$–10 (cf. $Sc \sim 100$–6000 for PMSE, e.g., Strelnikov and Rapp, 2011). This, however extends the structures in plasma constituents (their spectrum) to 2 to 3 times smaller scales than it is done by the pure neutral air turbulence, i.e. for neutral density (e.g., Asmus et al., 2017; Staszak et al., 2020).

The spectral function $S_{N_e}(k)$ in this case must be the one of the Batchelor (1959)'s theory. Its universal range spectrum must reveal three subranges: the inertial-convective ($k^{-5/3}$), viscous-convective (k^{-1}), and viscous-diffusive (k^{-7} or $\exp\{k^{-2}\}$). Fig. 1 demonstrates two universal range scalar spectra in turbulence field for the cases $Sc \gg 1$ and $Sc = 1$ in red and blue, respectively.

2.3.3. Small-scale waves theory of PMWE

Hocking et al. (1991) proposed a model for viscosity wave production in the atmosphere to explain specular radar reflections, assuming that the viscosity waves might be generated during reflection of gravity waves. In order to explain PMSE, they adapted the model to consider reflection of infrasound at steps of temperature or wind-shear, which would in turn generate viscosity waves of a scale suitable to reflect VHF radiowaves. They showed that radiowaves could be reflected from these viscosity waves with strength sufficient to explain PMSE.

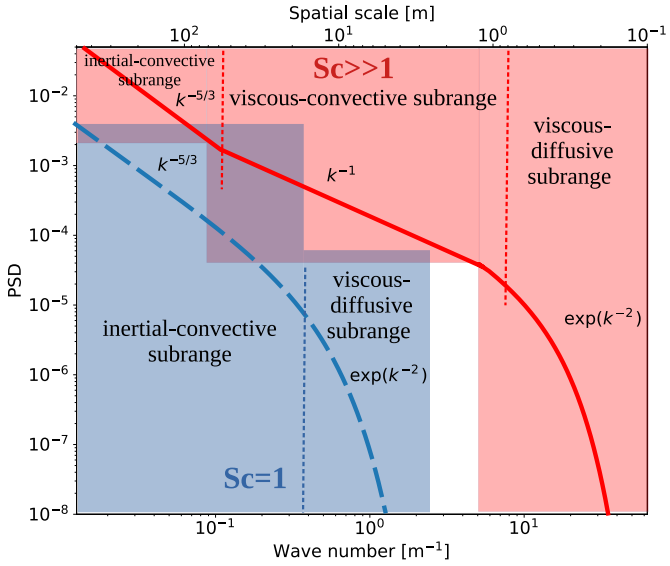

Fig. 1. Schematics showing universal range scalar spectra for Sc = 1 (blue dashed spectrum) and Sc¿¿1 (solid red spectrum). The red spectrum is described by the Batchelor (1959)'s theory and additionally reveals viscous-convective (k^{-1}) subrange. Vertical dashed lines mark separation between subranges.

Kirkwood et al. (2006b) proposed a similar explanation for PMWE. They observed highly aspect-sensitive echoes, which moved horizontally with the speed of sound. Their explanation was that damped ion-acoustic waves may lead to the creation of radar echoes. According to Hocking et al. (2016), these waves and the viscosity waves mentioned earlier are essentially the same. Recently, this hypothesis has been revisited and other mechanisms involving infrasound waves in the vicinity of caustics and turning points were proposed by Belova et al. (2020).

2.3.4. Theory: additional aspects

The available experimental data as well as the existence of different theoretical approaches suggest, that there can be different types of PMWE, depending on altitude and background conditions. An indirect evidence for such complex nature of winter echoes can also be inferred from the ion chemistry of the D-region. Thus e.g, ionospheric plasma composition dramatically changes below approximately 80 km altitude. Whereas above this height it mainly consists of free electrons and positive ions, below 80 km also negative ions become a significant charge carrier (e.g., Friedrich et al., 0000; Plane et al., 2014; Asmus et al., 2015; Baumann et al., 2015; Stude et al., 2020). Further below, starting at ∼ 60 km, also concentration of free electrons rapidly vanishes (e.g., Friedrich, 2016, and references therein). The main role in destruction of negative ions plays atomic oxygen (e.g., Turunen et al., 1996; Friedrich et al., 0000; Baumann et al., 2015). Therefore, except for the dynamical state of the D-region, in terms of mean values (background) and small-scale processes, also detailed knowledge of the ionospheric composition might be important for understanding the PMWE phenomenon.

3. Sounding rocket project PMWE

To address this uncertainty in our knowledge of the creation mechanism of PMWE we initiated a self-titled sounding rocket project. The project involves two sounding rocket campaigns to be conducted at the north Norwegian Andøya Space Center (ASC, 69 ◦N, 16 ◦E). Two instrumented sounding rockets are to be launched in each campaign. The launch criterion is observation of PMWE by MAARSY on the path of the pre-calculated rocket trajectory. The launch window is planned based on the PMWE statistics by Latteck and Strelnikova (2015) updated by the additional observational seasons since that publication date. This statistics suggests that the highest probability to observe PMWE is around local noon.

The rocket instrumentation is configured so that the both turbulent and dusty-turbulent theories of PMWE can be tested based on in situ measurements. Also, the prerequisite conditions for the generation of the small-scale viscosity or ion-acoustic waves and composition of the ionosphere will be measured by the rocket-borne instruments.

Table 1
FIONA payload instrumentation.

Instrument	Institution	Parameter measured	References
CONE-NP (ionization gauge)	IAP	neutral density	Giebeler et al. (1993); Strelnikov et al. (2013)
CONE-EP	IAP	electron density	Skjelvan (1994)
MSPD	IAP	charged MSP density	Giono et al. (2018); Staszak et al. (2017)
MSPD negative grid	IAP	positive ion density	Staszak et al. (2017)
PD (Faraday cup)	IAP	charged MSP density	Asmus et al. (2013, 2017)
PD negative grid	IAP	positive ion density	Asmus et al. (2013, 2017)
ROMARA (ion mass spectrometer)	LMU/IPA	ion composition and charged MSP density	Stude et al. (2020)
Wave propagation experiment	TUG	absolute electron density	Bennett et al. (1972); Friedrich (2016)
PIP	IAP	positive ion density	Blix et al. (1990)
FIPEX	IRS	atomic oxygen density	Eberhart et al. (2015, 2019)
PaT	MISU	charged MSP density	Gumbel et al. (1997)

Table 2
DUSTIN payload instrumentation.

Instrument	Institution	Parameter measured	References
CONE-NP (ionization gauge)	IAP	neutral density	Giebeler et al. (1993); Strelnikov et al. (2013)
CONE-EP	IAP	electron density	Skjelvan (1994)
MSPD	IAP	charged MSP density	Giono et al. (2018); Staszak et al. (2017)
MSPD negative grid	IAP	positive ion density	Staszak et al. (2017)
PD (Faraday cup)	IAP	charged MSP density	Asmus et al. (2013, 2017)
PD negative grid	IAP	positive ion density	Asmus et al. (2013, 2017)
ECOMA	LMU/IPA	charged and neutral MSP density	Rapp and Strelnikova (2009)
Turb3D-NP (ionization gauge)	IAP	neutral density	Strelnikov et al. (2015)
Turb3D-EP	IAP	electron density	Strelnikov et al. (2015)
Wave propagation experiment	TUG	absolute electron density	Bennett et al. (1972); Friedrich (2016)
PIP	IAP	positive ion density	Blix et al. (1990)
FIPEX	IRS	atomic oxygen density	Eberhart et al. (2015, 2019)
Albedo photometers	MISU	upwelling radiation	Gumbel et al. (2020)

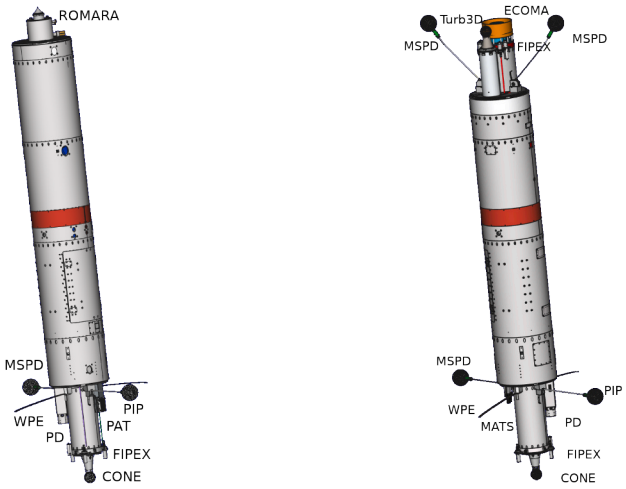

(a) FIONA payload (b) DUSTIN payload.

Fig. 2. PMWE payloads.

The parameters to be measured include background temperature of the neutral atmosphere as well as densities of the neutrals and all plasma species, i.e. electrons, ions, and MSP. All densities have to be measured with high spatial resolution and precision, so that also their fluctuations can be analyzed. The entire instrumentation was split between two payloads. The full list of the instruments and measured parameters is summarized in Tables 1 and 2 and Fig. 2 shows the both payloads with their instrumentation exposed to the atmosphere. One payload is equipped with the ion mass spectrometer ROMARA (Stude et al., 2020) whereas the other with the unique MSP detector ECOMA (Rapp and Strelnikova, 2009; Rapp et al., 2009, 2011b; Strelnikova et al., 2009a; Strelnikov et al., 2009; Strelnikov and Rapp, 2011). This gave rise to the

names FIONA and DUSTIN for these payloads to emphasize the focus on detailed ion and dust measurements, respectively.

Apart from this instrumentation, both payloads were equipped with the CONE instruments (Giebeler et al., 1993; Skjelvan, 1994; Strelnikov et al., 2013). CONE stands for COmbined measurements of Neutrals and Electrons, that is it measures neutral and electron number densities with high altitude resolution and precision. The neutral density measurements yield absolute number density (making use of laboratory calibration), neutral temperature (by integration assuming hydrostatic equilibrium), and turbulence energy dissipation rate profiles (from spectral analysis of density fluctuations, e.g., Lübken, 1992; Lübken et al., 1993; Lübken, 1997; Strelnikov et al., 2003, 2013). The electron density measured by the CONE only yield relative densities and density fluctuations. To properly characterize plasma behavior connected to PMWE, both payloads were equipped with Positive Ion Probes (PIP) and novel MSP detectors (MSPD, Staszak et al., 2017; Giono et al., 2018).

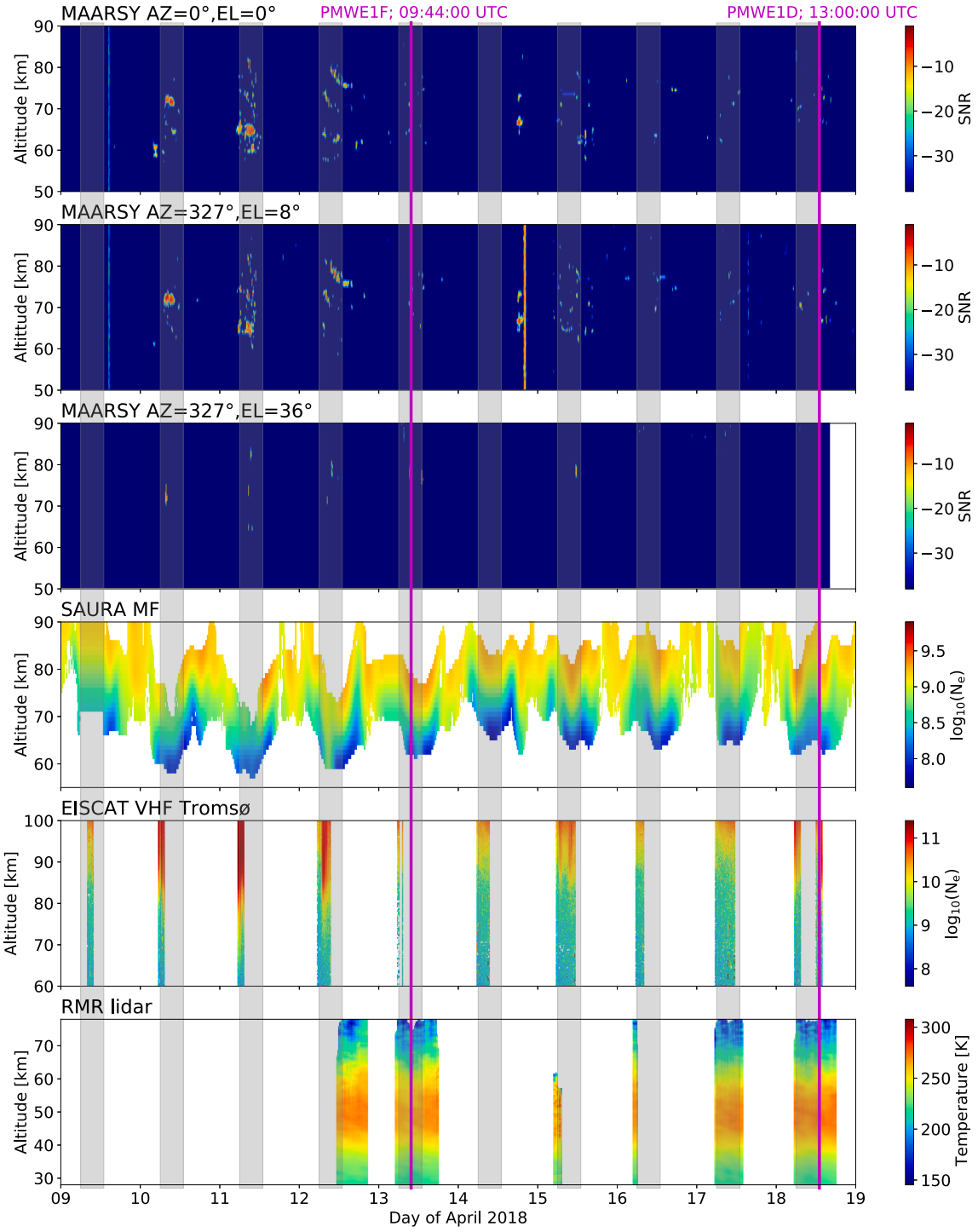

Fig. 3. Launch conditions during the PMWE-1 rocket campaign. From top to bottom: Upper three panels show PMWE display observed by MAARSY's vertical, upleg, and downleg beams; The 4th panel shows smoothed electron density observed by the Saura partial reflection radar; The 5th panel shows ESCAT electron density measurements; The lower panel shows temperature measurements by the RMR lidar. Grey shading shows launch windows for every day and the magenta lines mark rocket launch times. See text for details.

Both sensors aimed at measuring densities with high resolution and precision so that also fluctuation analysis can be accomplished. The particle detector (PD) based on the Faraday cup measurement principle is also mounted on the rear deck of both payloads. This instrument was successfully applied for MSP studies in previous sounding rocket projects (Asmus et al., 2013, 2017). Since the absolute level of ionization is crucial for understanding the PMWE phenomenon the wave propagation experiment (WPE) is integrated in both payloads (Bennett et al., 1972; Friedrich, 2016). Also, both payloads carry several FIPEX sensors for atomic oxygen density measurements with high altitude resolution (Eberhart et al., 2015, 2019).

The rear deck of the FIONA payload is equipped with the particle detector PaT (Gumbel et al., 1997), whereas the DUSTIN payload carries two different versions of the MSPD instrument. Additionally, a pair of albedo photometers are mounted on the rear deck of the DUSTIN payload. These downward-viewing instruments measure contributions of upwelling radiation to the illumination of the mesosphere (Gumbel et al., 2020).

A simplified version of the next generation ionization gauge CONE developed for three dimensional soundings of mesospheric turbulence, the Turb3D instrument (Strelnikov et al., 2015) is mounted on the front deck of the DUSTIN payload.

Also, both payloads contained several new technological developments by the Mobile Rocket Base (MORABA) of the German Aerospace Center DLR. Some of those developments included a new advanced telemetry system, Kodiak GNSS receiver with integrated navigation experiments, and a new sea recovery system (Göser et al., 2019).

The Arctic Lidar Observatory for Middle Atmosphere Research (ALOMAR, von Zahn et al., 1995) is located close the launch site and is an integral part of the entire PMWE mission. All radars and lidars that contribute to the ALOMAR are running in a dedicated campaign mode to support in situ measurements.

4. PMWE-1 rocket campaign

In April 2018 the first sounding rocket campaign PMWE-1 was successfully conducted at the ASC. The payloads were launched on two separate days and the flights were labeled PMWE1F (PMWE-1 campaign, FIONA payload) and PMWE1D (PMWE-1 campaign, DUSTIN payload). Apart from MAARSY and Saura (Rapp et al., 2011a; Latteck et al., 2012; Singer et al., 2008), the ground support also included the ESRAD MST (e.g., Kirkwood et al., 2006a), and the EISCAT VHF radars (Baron, 1986). The IAP RMR lidar at ALOMAR continuously operated whenever weather conditions permitted.

The launch window was opened on 9th of April and scheduled for 08:00 to 15:00 LT. Starting from 10th of April and during the next three days MAARSY detected quite long-lasting PMWE, however weather conditions prohibited rocket launches because of safety requirements. Also the EISCAT VHF and Saura partial reflection radars detected slightly enhanced ionization during PMWE observations. The first possibility to launch a PMWE payload due to the launch safety occurred on 13 of April. Fig. 3 shows an overview of the launch conditions during the entire campaign period. Vertical grey shaded stripes show times of the launch window and the two rocket launches are marked by the vertical magenta lines. The three upper panels in Fig. 3 show the PMWE display as observed by three MAARSY beams during the campaign period. The two north-west directed beams at azimuth of 327 ◦ and elevations of 8 ◦ and 36 ◦ (from vertical) were measuring in a common volume with the in situ soundings on rocket's up- and downleg, respectively. The fourth panel from top in Fig. 3 shows smoothed measurements of electron densities by the Saura radar. The bottom edge of these data is due to the lower sensitivity limit of the radar. The upper edge of these Saura measurements is due to an enhanced ionization which makes unambiguous derivation of N_e very difficult. This plot nicely shows the diurnal cycles of the ionization of the lower ionosphere. The next panel shows electron density measurements by the EISCAT VHF radar. This radar is only sensitive to higher N_e values and, therefore its measurement range lies above those of the Saura radar. Note, that EISCAT only operated during few hours per day. Both panels with N_e measurements demonstrate the change of ionization level of the lower ionosphere during the campaign period. The lower panel of Fig. 3 shows temperature measurements by the RMR-lidar.

Fig. 3 basically demonstrates that the best scientific conditions were present during the first days of the campaign period when, however, weather conditions prohibited the rocket launch. Both ESRAD and EISCAT radars did not see any PMWE during the entire campaign period. This is consistent with the quite low ionization level of the lower ionosphere.

The low and stable ionization level of the ionosphere must be considered an advantage for our project since the mission's goal is to investigate PMWE creation mechanism. It is well known that the main prerequisites for PMWE observation are 1) presence of small-scale structures in electron density and 2) level of the background ionization (background N_e) must exceed a certain (radar-specific) threshold. High ionization level of the D- and lower E-regions, normally caused by either high solar activity or geomagnetic disturbances is very dynamic on relatively short time scales. That is e.g., during particle precipitation events electron densities can change by about order of magnitude within a few seconds (e.g., Kirkwood and Osepian, 1995). This decreases stability of the main contributors to PMWE formation.

4.1. PMWE1F (FIONA) launch

On 13 of April 2018 soon after the opening of launch window thin PMWE layers were detected by the vertical MAARSY beam. Then they were seen in the 8 ◦ tilted beam that was directed along the ascending part of rocket trajectory. When some echo also appeared in the display of the 36 ◦ tilted beam, that is on the rocket's downleg, the decision was made to launch the FIONA payload. The MAARSY PMWE observations by the three beams during the launch of the PMWE1F payload are shown in Fig. 4. The PMWE1F payload was launched on 13 of April 2018 at 09:44:00 UTC. The 8 ◦ tilted beam also registered reflection from the payload which is seen as a vertical line of strong radar echo. Similar signatures can also be seen in the downleg beam, but only between ∼ 68 and 80 km. This line nicely confirms the intersection of the MAARSY beam and the rocket trajectory.

There are several features apparent in Fig. 4. First of all, the echoes observed during this day are relatively weak in general. It is seen that the lower PMWE (i.e. below ∼ 70 km) appear as very thin layers (1–2 range gates) that stay long time at near the same altitude. The downleg beam is either insensitive to the weak PMWE or echoes are spatially localized over zenith or even further to the south-east, i.e. to the other side of the vehicle's flight path area. The only PMWE signature in the downleg beam that appears shortly before rocket launch is smeared over almost 5 km and lasts only a few minutes. Another noteworthy feature seen in the upleg display appears right after the rocket passage through the radar beam. It is seen, that new radar echoes artificially created by the passage of the rocket were created at approximately 75 and 79 km. Then these echoes were advected vertically by ∼ 3 range gates and are seen in this beam for 3–5 min. The upper artificial echo looks like an extension of the natural echo observed before and during the rocket launch and is much stronger than the lower one. Then, the upper artificial echo drifted horizontally southwards and subsequently appears in vertical and in southwards tilted (azimuth = 87 ◦, tilt = 8 ◦, not shown here) beams.

4.2. PMWE1F (FIONA) measurements

Latteck et al. (2019) show details of MAARSY and Saura observations during the PMWE-1 campaign. A detailed analysis of the in situ measurements conducted during the PMWE1F rocket flight is given in the companion paper by Staszak et al. (2020). The mass spectrometer

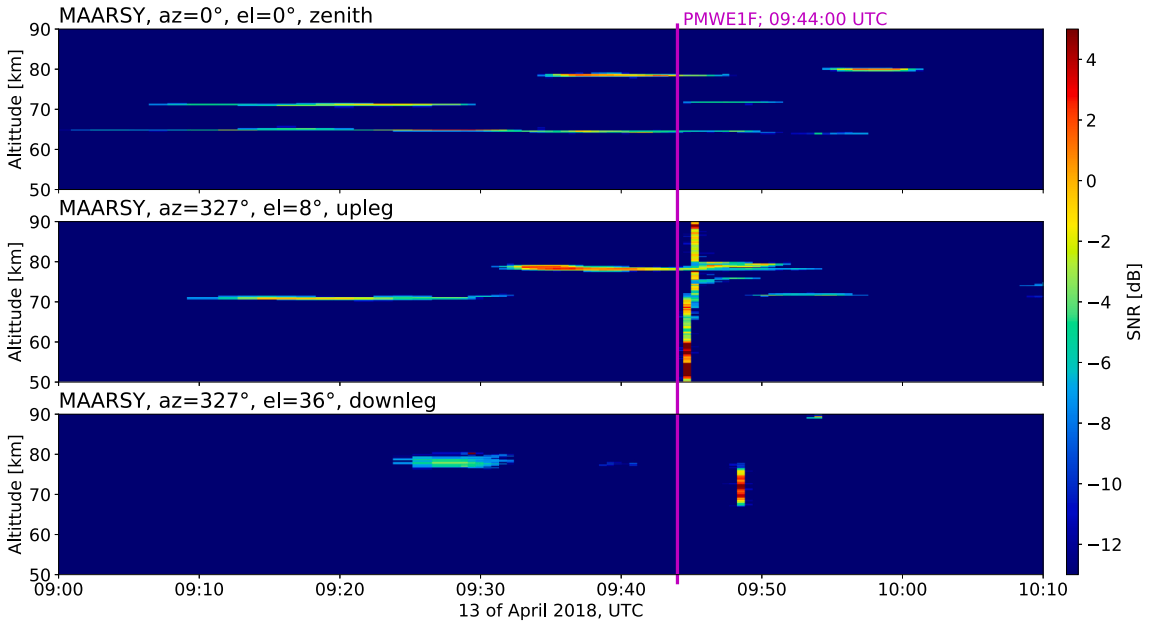

Fig. 4. PMWE display observed by MAARSY during day of FIONA payload launch (PMWE1F). The panels from top to bottom: vertical beam, beam along the rocket ascend (8 ◦ elevation), beam crossing the rocket descend (36 ◦ elevation).

ROMARA on PMWE1F measured heavy negative ion signatures during ascent which is discussed by Stude et al. (2020). Here we briefly recapitulate the main findings of these studies. Staszak et al. (2020) together with Stude et al. (2020) show that MSP were detected on up as well as on the downleg of the PMWE1F flight. Also, Staszak et al. (2020) showed that the upper PMWE layer, i.e. at ∼ 80 km altitude, was created by neutral air turbulence. Staszak et al. (2020) also show that this upper turbulence layer was created by breaking gravity waves. Their analysis is consistent with the behavior of radar echoes described in detail by Latteck et al. (2019). Also, the lower PMWE layers (i.e., below 75 km) were co-located with turbulence layers. Since both lower PMWE and turbulence were quite weak, the authors did not draw such solid conclusions as for the upper layer, but only noticed the similarity with the upper turbulent PMWE.

4.3. PMWE1D (DUSTIN) launch

After the successful launch of the PMWE1F payload, no further PMWE was observed which were strong enough for a valuable launch of the second instrumented payload. The detected echoes when they appeared were very weak, low, and short lived, i.e. less than 10 min duration (see Fig. 3). The echoes below approximately 70 km are essentially difficult to investigate in situ due to aerodynamics of the rocket flight (see e.g., Gumbel, 2001; Hedin et al., 2007; Strelnikova et al., 2009b; Staszak et al., 2015). Since no suitable scientific conditions were met until the end of the planned (and therefore, funded) launch window, the decision was made to launch on the very last minute. The main reason for this was that the DUSTIN payload was equipped with numerous novel instruments and service module (see Sec. 3) that required at least a technological test. Such a technological test was

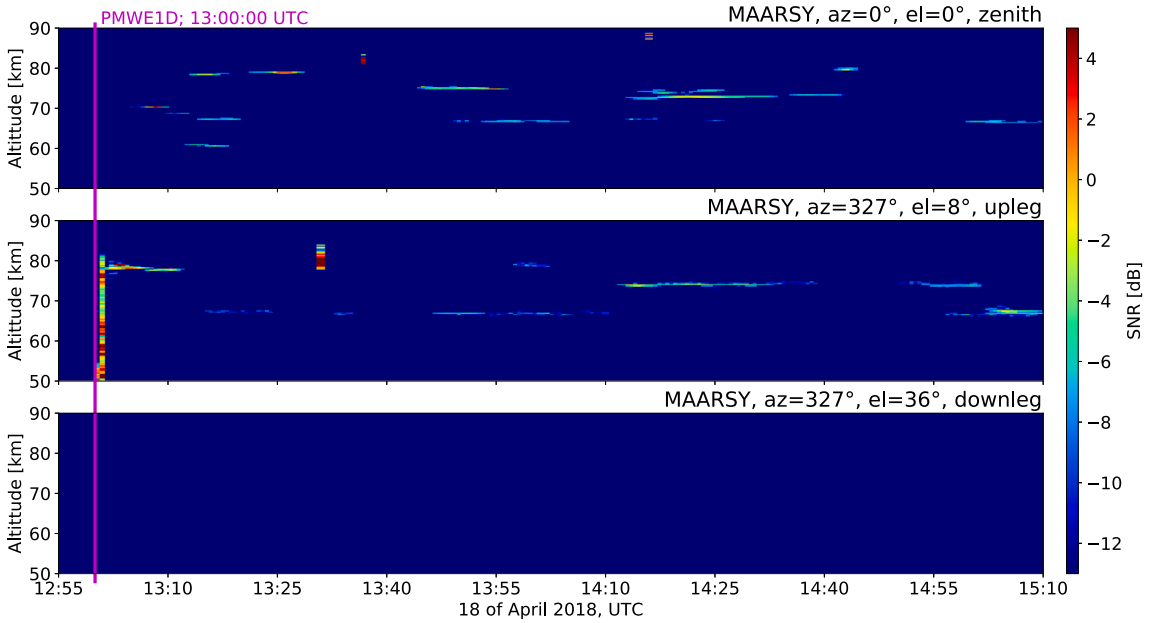

Fig. 5. MAARSY PMWE display observed during the day of PMWE1D (DUSTIN) launch.

important for the entire PMWE program to assure the best payload performance during the second field campaign planned to be conducted in October 2021.

The second payload PMWE1D (DUSTIN) was launched on 18 of April 2018 at 13:00:00 UTC. No radar echo was seen by MAARSY, all the more so by the ESRAD and EISCAT. The PMWE display monitored by MAARSY is shown in Fig. 5.

4.4. PMWE1D (DUSTIN) measurements

As in the first case of the PMWE1F launch, MAARSY tracked the main payload by the 8 ◦ tilted beam. Remarkably, a strong artificial radar echo was also created by the PMWE1D payload at ∼ 78 km height. Shortly after the rocket launch both Saura partial reflection and EISCAT VHF radars started to observe an enhancement of the background ionization. Expectedly, some radar echoes also appeared on the MAARSY PMWE display. Figs. 6 and 7 show evolution of electron density close to the PMWE1D launch time, measured by the Saura and EISCAT radars, respectively. The color scales are the same as in Fig. 3.

As mentioned in Sec. 4, the PMWE1D payload carried a new generation CONE instrument named Turb3D. Combined measurement results (i.e., by Turb3D and RMR lidar) of the background density and temperature fields are shown in Figs. 8 and 9, respectively. The measured neutral air density field does not reveal noticeable variations within the altitude range of the PMWE occurrence, i.e. between 60 and 80 km. However, it is apparent that the temperature field above ∼ 60 and up to ∼ 105 km is strongly affected by atmospheric waves.

Rocket-borne measurements of the turbulence field on board the PMWE1D payload are shown in Fig. 10. They only reveal three thin and weak layers at 65, 70 and 80 km altitude. These turbulence layers are 200–300 m in thickness and reveal energy dissipation rates close to the theoretical minimum of $\varepsilon_{min} = \nu \cdot \omega_B^2$ shown by the dashed line in Fig. 10 (ω_B is the Brunt-Väisälä frequency). The green and yellow symbols with error bars show results of turbulence analysis applying two different spectral models (see e.g., Strelnikov et al., 2013, for details). The difference in these ε-values should be considered as method's uncertainty.

Finally, in Fig. 11 we show results of measurements of neutral MSP density by the ECOMA particle detector. Fig. 11 shows three altitude-profiles of the photo-currents measured on downleg of the PMWE1D rocket flight.

These currents are produced by photo-electrons emitted from the MSP when they are irradiated by the flash lamps of the ECOMA instrument (Rapp and Strelnikova, 2009). The strongest signal results from

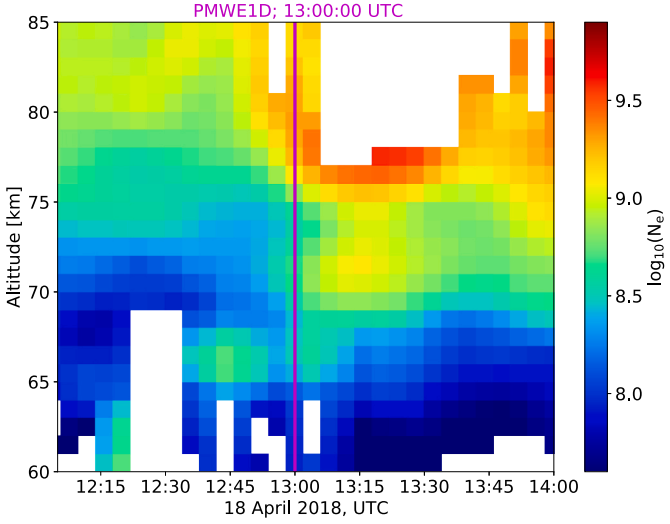

Fig. 6. Electron density observed by the Saura partial reflection radar. The magenta line marks PMWE1D rocket launch time.

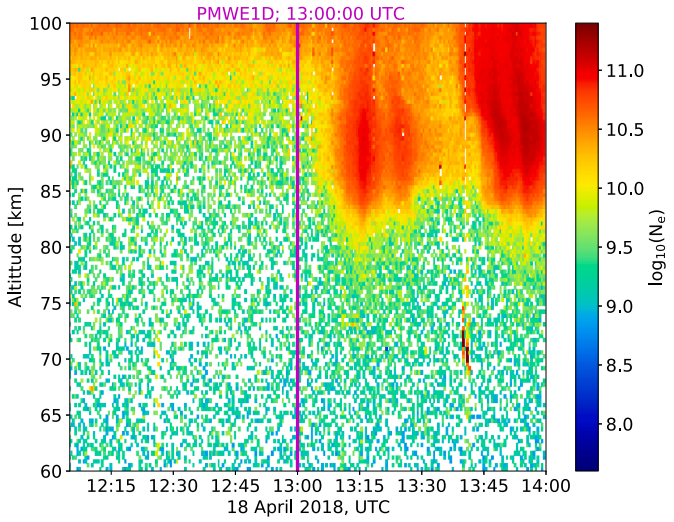

Fig. 7. EISCAT electron density measurements. The magenta line marks PMWE1D rocket launch time.

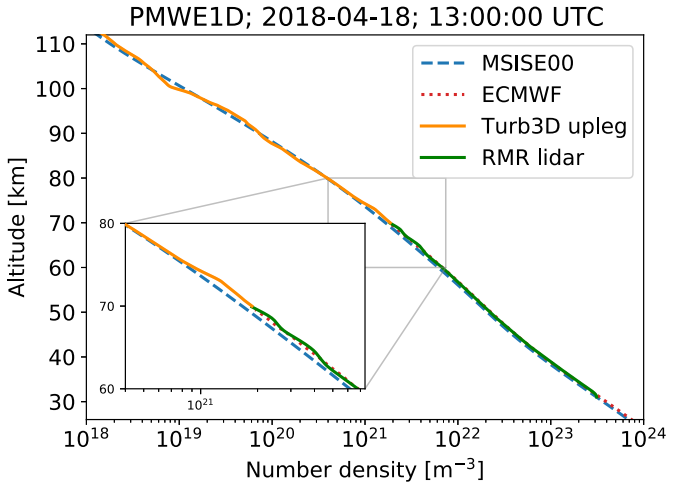

Fig. 8. Neutral air density measured by the Turb3D ionization gauge (orange profile) and RMR lidar (green profile). Solid blue and dotted red lines show reference density profiles from NRL-MSISE00 and ECMWF, respectively.

the ionization of MSP by the lamp FX1162 which emits photons with energies of ∼ 11 eV (blue profile in Fig. 11). To convert these currents into MSP number density an assumption about MSP material (its work function) must be made. This will introduce large uncertainties because of lack of our knowledge of the MSP composition. Such a conversion needs a detailed description and treatment of numerous aspects which are beyond the scope of this paper. Nevertheless, these data are consistent with the earlier ECOMA measurements (Rapp et al., 2011b) and show that MSP were present in the MLT below ∼ 100 km in an amount typical for winter conditions.

5. Discussion

The first sounding rocket campaign PMWE-1 conducted in April 2018 yielded some new observations and immediately allowed for at least a consistency check of the existing PMWE theories.

In the companion paper Staszak et al. (2020) show that the upper PMWE layer observed during PMWE1F flight, i.e. at ∼ 78 km altitude, was produced by a turbulent structure which moved together with gravity wave phase speed in direction approximately south-east. The drift direction was inferred from subsequent detection of similar

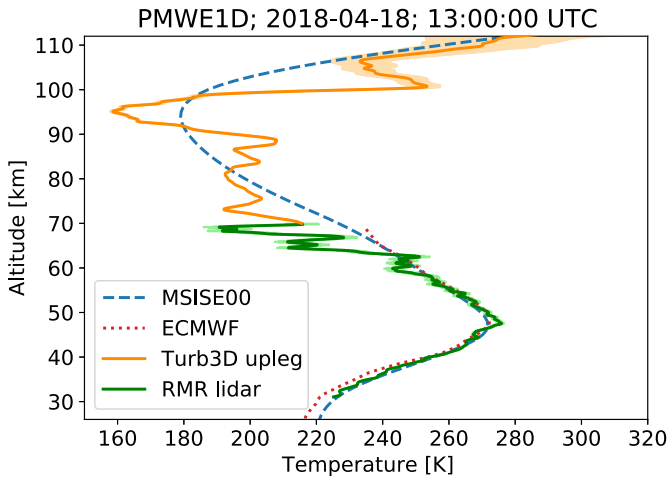

Fig. 9. Neutral temperature measured by the Turb3D ionization gauge (orange profile) and RMR lidar (green profile). Lidar data was integrated over 30 min and 1 km. Solid blue and dotted red lines show reference temperature profiles from NRL-MSISE00 and ECMWF, respectively.

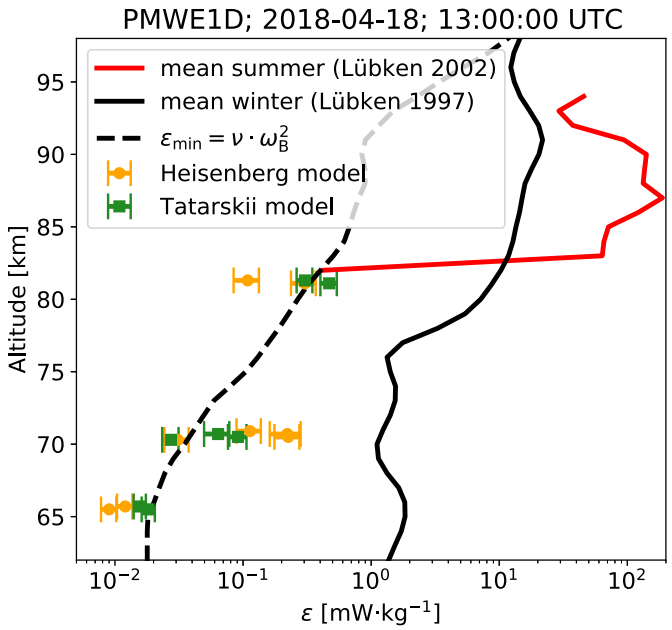

Fig. 10. Turbulence energy dissipation rates measurements by the Turb3D ionization gauge. The bold solid red and black profiles show turbulence climatology for summer and winter, respectively. The black dashed line shows minimum energy dissipation rates derived as $\varepsilon_{min} = \nu \cdot \omega_B^2$.

structures at the same altitudes in different radar beams. After applying the same observational technique to the lower PMWE layers observed during PMWE1F flight we can see that they drifted in the opposite direction. RMR-lidar measurements at ALOMAR show that different GWs observed at a fixed location can propagate in very different (and also opposite) directions (Strelnikova et al., 2020). That is, such opposite drift direction of lower PMWEs does not contradict the conclusions made by Staszak et al. (2020), but is rather in accord with it. Such advection of the turbulent structures at different heights by a front of GWs propagating in different (even opposite) directions can also explain why the lower artificial echo (i.e. that one observed during the PMWE1F launch at ~ 75 km) does not appear in the vertical radar beam as it does the upper artificial echo. The upper artificial echo reveals the same drift direction as its upper natural counterpart. This drift direction made it

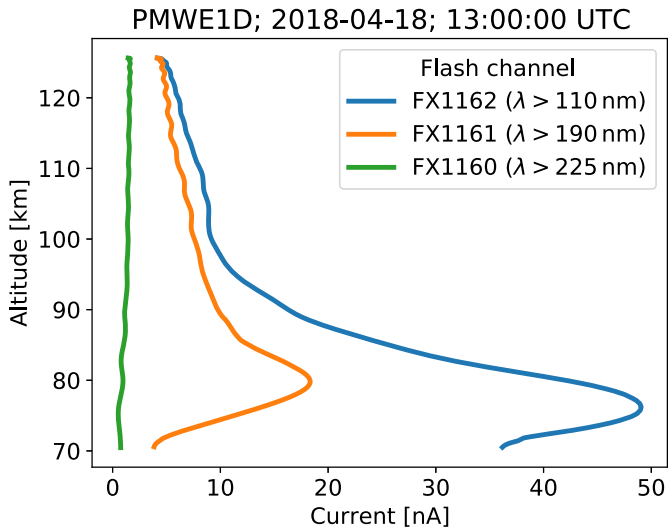

Fig. 11. MSP measurements by the flash channels of the ECOMA particle detector.

possible to subsequently observe this echo by several radar beams involved in the experiment, whereas the opposite drift direction (when starting point was the upleg looking radar beam) was not observable in that experiment configuration.

Owing to several technical issues, our rocket-borne measurements were not sensitive enough to resolve tiny amplitudes of the small-scale structures in densities of all plasma constituents inside the PMWE layers. However our well established and very sensitive technique to measure neutral density fluctuations by ionization gauges CONE, yielded measurements of turbulence parameters. These measurements revealed, that all PMWE layers occurred at altitudes where turbulence layers were observed by the rocket-borne instruments. This fact is well pronounced for the PMWE1F rocket flight (see Staszak et al., 2020, for details) and very suggestive when comparing turbulence measurements on board the PMWE1D payload and radar echoes following several minutes later. The layers of turbulent structures and of PMWE observed during PMWE1F launch revealed very similar altitudinal distribution and vertical extent. Turbulence measurements on board the second payload, PMWE1D, also showed thin layers which resemble PMWE layering observed several minutes later after the rocket sounding (i.e., when the background ionization increased). Since the last in situ and radar measurements were not simultaneous, it is not possible to draw solid conclusion based on those measurements. In other words, one out of two rocket experiments strongly supports the pure turbulence theory of PMWE formation, whereas the second one only suggests a consistency with this theory.

Both ROMARA measurements on PMWE1F payload (Stude et al., 2020) and ECOMA measurements on board the PMWE1D payload, as well as the earlier in situ measurements (see e.g., Baumann et al., 2013; Robertson et al., 2014), show that dust particles are an integral part of the winter MLT. That is, MSP are always present in the winter polar mesosphere. However, Staszak et al. (2020) show that the ambient MSP only play minor role by extending the small-scale N_e-structures to slightly smaller scales. Owing to tiny sizes of MSP (1 nm and less) this spectral extension is relatively small (i.e., much less than decade).

Hocking (2003) reviewed radar observations of thin layers of partial reflections at frequencies 2–50 MHz and presented a hypothesis that they may be due to diffusive waves of various types present in laminar regions of the atmosphere. Kirkwood et al. (2006b) applied this theory to explain the formation of strong or very strong PMWE. This theory explains radar echoes when no turbulence is generated in the mesosphere. Observations of turbulence instead of laminar regions at PMWE altitudes during PMWE-1 rocket campaign does not generally contradict

the hypothesis made by Hocking et al. (1991), Hocking (2003), and Kirkwood et al. (2006b). In accord with commonly accepted knowledge our in situ measurements show that also inside PMWE layers turbulence is very intermittent (Staszak et al., 2020). That is it reveals adjacent regions of strong and very weak dissipation (and therefore turbulence intensity) and also some laminar flow regions (i.e., where no turbulence was detected by a rocket-borne instrument). That is, even though our in situ turbulence measurements do not support the hypothesis of viscous waves as PMWE creation mechanism, they also cannot rule it out.

On the other hand, such layers of partial reflections must be accompanied by sharp gradients in physical quantities that define the refractive index of the atmosphere (Hocking et al., 1991; Hocking, 2003). Such gradients must arise in regions of laminar flow adjacent to turbulent layers (Hocking et al., 1991). For observations of radar echoes from the mesosphere the most important parameter that defines the refractive index is electron density. Our in situ measured N_e-profiles, do not reveal such layers below 80 km altitude. They rather show a decreased gradient in the region of PMWE occurrence, i.e. an almost vertical line (Staszak et al., 2020). Also the measured neutral density profiles behave similarly, i.e. do not reveal sharp gradients at PMWE altitudes (see also Fig. 8). In other words, the prerequisites for a possible connection between small-scale viscous waves and PMWE were not observed by the rocket-borne instruments.

On the other hand, all the PMWE observed during this rocket campaign revealed relatively low SNR and volume reflectivity, whereas the small-scale waves theory is rather suitable for strong echoes. Also, as discussed above, the radar echoes observed near 80 and below 70 km altitude reveal somewhat different properties, e.g., strength, vertical extent, duration. In other words, as mentioned in Sec. 2.3.4 and suggested by the results of PMWE-1 sounding rocket campaign, there could be different types of PMWE having different creation mechanisms.

A very striking event accompanied both rocket launches was the creation of artificial echoes by both payloads. The first payload, PMWE1F created two echoes at $\sim$ 75 and 79 km altitude, whereas the second payload, PMWE1D only created one artificial echo at $\sim$ 79 km. The behavior of these upper artificial echoes in both cases is very similar. That is, they revealed very narrow spectral width and high SNR (Latteck et al., 2019), after creation they were slightly advected vertically and drifted horizontally in the same direction as the natural PMWE observed at those altitudes. In the case of PMWE1F flight, it was shown by Staszak et al. (2020), that they were moving with the phase speed of gravity waves propagating in the background atmosphere. Also, the artificial echo during PMWE1F launch was formed at an altitude where the natural PMWE was observed. In approximately 1 h after the PMWE1D flight, natural PMWE also appeared at the same altitude. These facts suggest that at the certain heights there were some favorable conditions for formation of artificial echoes. The exact reason for the formation and nature of the artificial echoes is not clear yet. Currently we are revising all the factors and flight conditions that could shed light on the nature of these artificial echoes and plan for publishing a separate paper on this topic.

6. Summary

The first sounding rocket campaign dedicated to investigation of Polar Mesosphere Winter Echoes (PMWE) was successfully conducted from the north Norwegian Andøya Space Center (ASC) in April of 2018. The first sounding rocket PMWE1F was launched into decaying PMWE structure and yielded measurements of small-scale structures in densities of neutrals and electrons, as well as of background temperatures and densities. Ground-based instruments continuously measured background winds, temperature, and electron density several hours around the rocket launch time. This set of data allows to precisely characterize the background and to derive the radar volume reflectivity based on instant measurements. Since most of the measurements were made in a common volume with radar soundings, this allows for a direct comparison of PMWE structures and physical quantities involved in creation of this phenomenon.

MSP measurements made by different instruments onboard the both payloads (i.e., ROMARA analyzed by Stude et al. (2020), ECOMA, and plasma density fluctuations shown in Staszak et al. (2020)) show that tiny dust particles ($\lesssim$1 nm) are always present in the winter northern MLT. This is consistent with previous measurements.

Detailed analysis of measurements conducted during PMWE1F flight presented by Staszak et al. (2020) shows that the observed PMWE were created by neutral air turbulence. It also shows that charged dust particles were present in the PMWE layers, although their role was just to increase echo power. The same role was also played by the background ionization, i.e. by the ambient electron density. This data set is a first direct confirmation of the turbulent theory for PMWE formation.

The second rocket launch (PMWE1D) was made into no PMWE conditions and yielded similar set of measurements. However, several minutes later after the rocket flight, increased background ionization enlightened some radar echoes. These measurements allow to investigate the prerequisite conditions for PMWE formation. In situ measurements show that turbulence was present at altitudes where PMWE occurred which is in agreement with the results inferred from the first rocket launch. However, to precisely compare the radar echoes and rocket-borne measurements, real common volume and simultaneous measurements are needed. Therefore, the measurement results from the PMWE1D flight only indirectly support the turbulent theory of PMWE formation.

All turbulence and PMWE measurements conducted during PMWE-1 campaign consistently suggest that turbulence was responsible for creation of these radar echoes. Turbulence data together with the background observations suggest that the source of these turbulent structures was likely breakdown of gravity waves.

Since also in these rocket-borne measurements turbulence reveals high intermittency, this data does not contradict the other theory of PMWE formation, namely by the small-scale viscosity waves suggested by Hocking et al. (1991); Hocking (2003), and Kirkwood et al. (2006b). However, detailed investigation of all the density and temperature profiles did not yield any sharp gradient in the regions of PMWE occurrence, needed to support this theory.

To summarize, our measurements ultimately show that the polar winter mesosphere is abounded with MSP and intermittent turbulent layers. At altitudes below $\sim$ 85 km and down to $\sim$ 75 km turbulence creates small-scale structures in all the D-region constituents, including free electrons. When the background ionization is strong enough, these structures become visible for VHF radars.

Our measurements cannot exclude possibility, that PMWE observed below $\sim$ 75 km altitude may additionally reveal other creation mechanisms. These measurements also cannot shed light on another physical process which may affect the small-scale structures that cause the VHF radar echoes. These results, however, will be used to improve the quality of our measurement for the next rocket campaign.

A new striking event during this campaign was the creation of artificial radar echoes by both sounding rockets. These echoes revealed somewhat different properties and will be studied in more detail in a forthcoming paper.

Declaration of competing interest

The authors declare that they have no known competing financial interests or personal relationships that could have appeared to influence the work reported in this paper.

Acknowledgements

This work was supported by Federal Ministry for Economic Affairs and Energy on the basis of a decision by the Gernan Bundestag (DLR grant 50OE1402, project PMWE). The authors thank DLR-MORABA for

their excellent contribution to the project by developing the complicated PMWE payload and campaign support together with the Andøya Space Center, as well as H.-J. Heckl, T. Köpnick, and company vH-S GmbH for building the rocket instrumentation. The Austrian participation was made possible by project P-26932 of the Austrian Science Funds. EISCAT is an international association supported by the re search councils of Norway, Sweden, Finland, Japan, China, and the United Kingdom.

References

Asmus, H., Robertson, S., Dickson, S., Friedrich, M., Megner, L., 2015. Charge balance for the mesosphere with meteoric dust particles. J. Atmos. Sol. Terr. Phys. 127, 137–149. https://doi.org/10.1016/j.jastp.2014.07.010 layered Phenomena in the Mesopause Region.

Asmus, H., Staszak, T., Strelnikov, B., Lübken, F.J., Friedrich, M., Rapp, M., 2017. Estimate of size distribution of charged MSPs measured in situ in winter during the WADIS-2 sounding rocket campaign. Ann. Geophys. 979 https://doi.org/10.5194/angeo-35-979-2017.

Asmus, H., Strelnikov, B., Rapp, M., 2013. In situ measurements of charged mesospheric ice particles during the PHOCUS 2011 campaign and comparison of the results with a microphysical model. In: 21nd ESA Symposium on European Rocket and Balloon Programmes and Related Research, pp. 489–493.

Baron, M., 1986. EISCAT progress 1983-1985. J. Atmos. Terr. Phys. 48, 767–772.

Batchelor, G.K., 1959. Small-scale variation of convected quantities like temperature in turbulent fluid: Part 1. General discussion and the case of small conductivity. J. Fluid Mech. 5, 113–133. https://doi.org/10.1017/S002211205900009X.

Baumann, C., Rapp, M., Anttila, M., Kero, A., Verronen, P.T., 2015. Effects of meteoric smoke particles on the D region ion chemistry. J. Geophys. Res.: Space Physics 120, 10823–10839. https://doi.org/10.1002/2015JA021927.

Baumann, C., Rapp, M., Kero, A., Ennell, C.F., 2013. Meteor smoke influences on the d-region charge balance - review of recent in situ measurements and one-dimensional model results. Ann. Geophys. 31, 2049–2062. https://doi.org/10.5194/angeo-31-2049-2013.

Baumgarten, G., Fiedler, J., Lübken, F.J., von Cossart, G., 2008. Particle properties and water content of noctilucent clouds and their interannual variation. J. Geophys. Res.: Atmosphere 113. https://doi.org/10.1029/2007JD008884. https://agupubs.onlinelibrary.wiley.com/doi/abs/10.1029/2007JD008884.

Belova, E., Kero, J., Näsholm, S.P., Vorobeva, E., Godin, O.A., Barabash, V., 2020. Polar mesosphere winter echoes and their relation to infrasound. EGU General Assembly. https://doi.org/10.5194/egusphere-egu2020-5055, 2020.

Bennett, F., Hall, J., Dickinson, P., 1972. D-region electron densities and collision frequencies from faraday rotation and differential absorption measurements. J. Atmos. Terr. Phys. 34, 1321–1335. https://doi.org/10.1016/0021-9169(72)90188-2. http://www.sciencedirect.com/science/article/pii/0021916972901882.

Blix, T.A., Thrane, E.V., Andreassen, Ø., 1990. In situ measurements of the fine-scale structure and turbulence in the mesosphere and lower thermosphere by means of electrostatic positive ion probes. J. Geophys. Res.: Atmosphere 95, 5533–5548. https://doi.org/10.1029/JD095iD05p05533. https://agupubs.onlinelibrary.wiley.com/doi/abs/10.1029/JD095iD05p05533.

Brattli, A., Blix, T.A., Lie-Svendsen, Ø., Hoppe, U.P., Lübken, F.J., Rapp, M., Singer, W., Latteck, R., Friedrich, M., 2006. Rocket measurements of positive ions during polar mesosphere winter echo conditions. Atmos. Chem. Phys. 6, 5515–5524.

Chen, F.F., 2016. Introduction to Plasma Physics and Controlled Fusion. https://doi.org/10.1007/978-3-319-22309-4.

Cho, J.Y.N., Hall, T.M., Kelley, M.C., 1992. On the role of charged aerosols in polar mesosphere summer echoes. J. Geophys. Res. 97, 875–886.

Cho, J.Y.N., Kelley, M.C., 1993. Polar mesosphere summer radar echoes: observations and current theories. Rev. Geophys. 31, 243–265. https://doi.org/10.1029/93RG01535. https://agupubs.onlinelibrary.wiley.com/doi/abs/10.1029/93RG01535.

Collis, P.N., Rietveld, M.T., Röttger, J., Hocking, W.K., 1992. Turbulence scattering layers in the middle-mesosphere observed by the EISCAT 224-MHz radar. Radio Sci. 27, 97–107. https://doi.org/10.1029/91RS02963.

Czechowsky, P., Rüster, R., Schmidt, G., 1979. Variations of mesospheric structures in different seasons. Geophys. Res. Lett. 6, 459–462.

Eberhart, M., Löhle, S., Steinbeck, A., Binder, T., Fasoulas, S., 2015. Measurement of atomic oxygen in the middle atmosphere using solid electrolyte sensors and catalytic probes. Atmospheric Measurement Techniques 8, 3701–3714. https://doi.org/10.5194/amt-8-3701-2015. https://www.atmos-meas-tech.net/8/3701/2015/.

Eberhart, M., Löhle, S., Strelnikov, B., Hedin, J., Khaplanov, M., Fasoulas, S., Gumbel, J., Lübken, F.J., Rapp, M., 2019. Atomic oxygen number densities in the mesosphere–lower thermosphere region measured by solid electrolyte sensors on WADIS-2. Atmospheric Measurement Techniques 12, 2445–2461. https://doi.org/10.5194/amt-12-2445-2019. https://www.atmos-meas-tech.net/12/2445/2019/.

Ecklund, W.L., Balsley, B.B., 1981. Long-term observations of the arctic mesosphere with the MST radar at poker flat, Alaska. J. Geophys. Res. 86, 7775–7780. https://doi.org/10.1029/JA086iA09p07775.

Fortov, V., Ivlev, A., Khrapak, S., Khrapak, A., Morfill, G., 2005. Complex (dusty) plasmas: current status, open issues, perspectives. Phys. Rep. 421, 1–103. https://doi.org/10.1016/j.physrep.2005.08.007. http://www.sciencedirect.com/science/article/pii/S0370157305003339.

Fortov, V.E., Khrapak, A.G., Khrapak, S.A., Molotkov, V.I., Petrov, O.F., 2004. Dusty plasmas. Phys. Usp. 47, 447–492 https://doi.org/10.1070doi:10.1070/pu2004v047n05abeh001689.

Friedrich, M., 2016. Handbook of the lower ionosphere. Verlag der Technischen universität graz. https://lampx.tugraz.at/karl/verlagspdf/ionosphere_friedrich_ebook.pdf.

Friedrich, M., Rapp, M., 2009. News from the lower ionosphere: a review of recent developments. Surveys in Geophyhsics 30, 525–559. https://doi.org/10.1007/s10712-009-9074-2.

Friedrich, M., Rapp, M., Plane, J.M., Torkar, Klaus M., d..j.g..a.i...j..J.k..B.m..s.n...p...p..E.t..B.u..h.v...y.

Gage, K., 1990. Radar Observations of the Free Atmosphere: Structure and Dynamics. American Meteorological Society, Boston, MA, pp. 534–565. https://doi.org/10.1007/978-1-935704-15-7_37.

Giebeler, J., Lübken, F.J., Nägele, M., 1993. Cone - a new sensor for in-situ observations of neutral and plasma density fluctuations. In: Proceedings of the 11th ESA Symposium on European Rocket and Balloon Programmes and Related Research, pp. 311–318.

Giono, G., Strelnikov, B., Asmus, H., Staszak, T., Ivchenko, N., Lübken, F.J., 2018. Photocurrent modelling and experimental confirmation for meteoric smoke particle detectors on board atmospheric sounding rockets. Atmospheric Measurement Techniques 11, 5299–5314. https://doi.org/10.5194/amt-11-5299-2018. https://www.atmos-meas-tech.net/11/5299/2018/.

Göser, J., Drescher, O., Hörschgen-Eggers, M., Gemeinhardt, U., 2019. Search and rescue: development and verification of a modernized passive floating system for payload sea recovery. In: 24th ESA Symposium on European Rocket & Balloon Programmes and Related Research. https://elib.dlr.de/131730/.

Gumbel, J., 2001. Aerodynamic influences on atmospheric in situ measurements from sounding rockets. J. Geophys. Res.: Space Physics 106, 10553–10563. https://doi.org/10.1029/2000JA900166. https://agupubs.onlinelibrary.wiley.com/doi/abs/10.1029/2000JA900166.

Gumbel, J., Megner, L., Christensen, O.M., Ivchenko, N., Murtagh, D.P., Chang, S., Dillner, J., Ekebrand, T., Giono, G., Hammar, A., Hedin, J., Karlsson, B., Krus, M., Li, A., McCallion, S., Olentšenko, G., Pak, S., Park, W., Rouse, J., Stegman, J., Witt, G., 2020. The mats satellite mission – gravity wave studies by mesospheric airglow/aerosol tomography and spectroscopy. Atmos. Chem. Phys. 20, 431–455. https://doi.org/10.5194/acp-20-431-2020. https://www.atmos-chem-phys.net/20/431/2020/.

Gumbel, J., Witt, G., Murtagh, D., Espy, P., Lundin, A., Wilhelm, N., Sundin, S., 1997. Noctilucent clouds and odd oxygen: results of the nlc-93 campaign. In: Kaldeich-Schürmann, B. (Ed.), 13th ESA Symposium on European Rocket and Balloon Programmes and Related Research, p. 483.

Hedin, J., Gumbel, J., Rapp, M., 2007. On the efficiency of rocket-borne particle detection in the mesosphere. Atmos. Chem. Phys. 7, 3701–3711.

Hervig, M.E., Gordley, L.L., Stevens, M.H., Russell III, J.M., Bailey, S.M., Baumgarten, G., 2009. Interpretation of SOFIE PMC measurements: cloud identification and derivation of mass density, particle shape, and particle size. J. Atmos. Sol. Terr. Phys. 316–330doi. https://doi.org/10.1016/j.jastp.2008.07.009.

Hocking, W.K., 2003. Evidence for viscosity, thermal conduction and diffusion waves in the earth's atmosphere (invited). Rev. Sci. Instrum. 74, 420–426. https://doi.org/10.1063/1.1516246.

Hocking, W.K., Fukao, S., Yamamoto, M., Tsuda, T., Kato, S., 1991. Viscosity waves and thermal-conduction waves as a cause of "specular" reflectors in radar studies of the atmosphere. Radio Sci. 26, 1281–1303. https://doi.org/10.1029/91RS01661. https://agupubs.onlinelibrary.wiley.com/doi/abs/10.1029/91RS01661.

Hocking, W.K., Röttger, J., Palmer, R.D., Sato, T., Chilson, P.B., 2016. Atmospheric Radar: Application and Science of MST Radars in the Earth's Mesosphere, Stratosphere, Troposphere, and Weakly Ionized Regions. Cambridge University Press. https://doi.org/10.1017/9781316556115.

Hoppe, U.P., Hall, C., Röttger, J., 1988. First observations of summer polar mesospheric backscatter with a 224 MHz radar. Geophys. Res. Lett. 15, 28–31. https://doi.org/10.1029/GL015i001p00028.

Hughes, D.W., 1997. Meteors and cosmic dust. Endeavour 21. https://doi.org/10.1016/S0160-9327(96)10030-2,31-35.

Janches, D., Heinselman, C.J., Chau, J.L., Chandran, A., Woodman, R., 2006. Modeling the global micrometeor input function in the upper atmosphere observed by high power and large aperture radars. J. Geophys. Res. 111 https://doi.org/10.1029/2006JA011628, 7317–+.

Kelley, M.C., Farley, D.T., Röttger, J., 1987. The effect of cluster ions on anomalous vhf backscatter from the summer polar mesosphere. Geophys. Res. Lett. 14, 1031–1034. https://doi.org/10.1029/GL014i010p01031. https://agupubs.onlinelibrary.wiley.com/doi/abs/10.1029/GL014i010p01031.

Kirkwood, S., Barabash, V., Belova, E., Nilsson, H., Rao, T., Stebel, K., Osepian, A., Chilson, P., 2002. Polar mesosphere winter echoes during solar proton events. Adv. Polar Up. Atmos. Res. 16, 111–125.

Kirkwood, S., Belova, E., Blum, U., Croskey, C., Dalin, P., Fricke, K.H., Goldberg, R.A., Manninen, J., Mitchell, J.D., Schmidlin, F., 2006a. Polar mesosphere winter echoes during MaCWAVE. Ann. Geophys. 24, 1245–1255. https://doi.org/10.5194/angeo-24-1245-2006.

Kirkwood, S., Chilson, P., Belova, E., Dalin, P., Häggström, I., Rietveld, M., Singer, W., 2006b. Infrasound - the cause of strong polar mesosphere winter echoes? Ann. Geophys. 24, 475–491. https://doi.org/10.5194/angeo-24-475-2006. https://www.ann-geophys.net/24/475/2006/.

Kirkwood, S., Osepian, A., 1995. Quantitative studies of energetic particle precipitation using incoherent scatter radar. J. Geomagn. Geoelectr. 47, 783–799. https://doi.org/10.5636/jgg.47.783.

Latteck, R., Renkwitz, T., Strelnikov, B., 2019. D region observations by VHF and HF radars during a rocket campaign at Andøya dedicated to investigations of PMWE. Adv. Radio. Sci. 17, 225–237. https://doi.org/10.5194/ars-17-225-2019.

Latteck, R., Singer, W., Bardey, H., 1999. The ALWIN MST radar: technical design and performance. In: Kaldeich-Schürmann, B. (Ed.), European Rocket and Balloon Programs and Related Research, p. 179.

Latteck, R., Singer, W., Rapp, M., Vandepeer, B., Renkwitz, T., Zecha, M., Stober, G., 2012. MAARSY: the new MST radar on Andøya-System description and first results. Radio Sci. 47, 1006. https://doi.org/10.1029/2011RS004775.

Latteck, R., Strelnikova, I., 2015. Extended observations of polar mesosphere winter echoes over Andøya (69°N) using MAARSY. J. Geophys. Res. 120, 8216–8226. https://doi.org/10.1002/2015JD023291.

Li, Q., Rapp, M., Röttger, J., Latteck, R., Zecha, M., Strelnikova, I., Baumgarten, G., Hervig, M., Hall, C., 2010. Microphysical parameters of mesospheric ice clouds derived from calibrated observations of polar mesosphere summer echoes at Bragg wavelengths of 2.8 m and 30 cm. J. Geophys. Res. 115, D00I13. https://doi.org/10.1029/2009JD012271.

Lie-Svendsen, O., Blix, T.A., Hoppe, U., Thrane, E., 2003. Modelling the plasma response to small-scale particle perturbations in the mesopause region. J. Geophys. Res. 108 (D8), 8442. https://doi.org/10.1029/2002JD002753.

Lübken, F.J., 1992. On the extraction of turbulent parameters from atmospheric density fluctuations. J. Geophys. Res. 97, 20,385-20,395.

Lübken, F.J., 1997. Seasonal variation of turbulent energy dissipation rates at high latitudes as determined by in situ measurements of neutral density fluctuations. Journal of Geophysical Research Atmospheres 102, 13441–13456. https://doi.org/10.1029/97JD00853.

Lübken, F.J., 1999. Thermal structure of the arctic summer mesosphere. J. Geophys. Res. 104, 9135–9149. https://doi.org/10.1029/1999JD900076.

Lübken, F.J., Hillert, W., Lehmacher, G., Von Zahn, U., 1993. Experiments revealing small impact of turbulence on the energy budget of the mesosphere and lower thermosphere. J. Geophys. Res. 98, 20369–20384. https://doi.org/10.1029/93JD02055.

Lübken, F.J., Rapp, M., Hoffmann, P., 2002. Neutral air turbulence and temperatures in the vicinity of polar mesosphere summer echoes. J. Geophys. Res. 107 (D15), 4273–4277. https://doi.org/10.1029/2001JD000915.

Lübken, F.J., Singer, W., Latteck, R., Strelnikova, I., 2007. Radar measurements of turbulence, electron densities, and absolute reflectivities during polar mesosphere winter echoes (PMWE). Adv. Space Res. 40, 758–764. https://doi.org/10.1016/j.asr.2007.01.015.

Lübken, F.J., Strelnikov, B., Rapp, M., Singer, W., Latteck, R., Brattli, A., Hoppe, U.P., Friedrich, M., 2006. The thermal and dynamical state of the atmosphere during polar mesosphere winter echoes. Atmos. Chem. Phys. 6, 13–24.

Mathews, J.D., Briczinski, S.J., Meisel, D.D., Heinselman, C.J., 2008. Radio and meteor science outcomes from comparisons of meteor radar observations at AMISR poker flat, søndrestrøm, and arecibo. Earth Moon Planets 102, 365–372. https://doi.org/10.1007/s11038-007-9168-0.

Morris, R.J., Klekociuk, A.R., Holdsworth, D.A., 2011. First observations of Southern Hemisphere polar mesosphere winter echoes including conjugate occurrences at 69°S latitude. Geophys. Res. Lett. 38, L03811. https://doi.org/10.1029/2010GL046298.

Nicolls, M.J., Kelley, M.C., Varney, R.H., J, H.C., 2009. Spectral observations of polar mesospheric summer echoes at 33 cm (450 MHz) with the poker flat incoherent scatter radar. J. Atmos. Sol. Terr. Phys. 71, 662–674.

Ottersten, H., 1969. Radar backscattering from the turbulent clear atmosphere. Radio Sci. 4, 1251–1255. https://doi.org/10.1029/RS004i012p01251.

Plane, J.M., Saunders, R.W., Hedin, J., Stegman, J., Khaplanov, M., Gumbel, J., Lynch, K. A., Bracikowski, P.J., Gelinas, L.J., Friedrich, M., Blindheim, S., Gausa, M., Williams, B.P., 2014. A combined rocket-borne and ground-based study of the sodium layer and charged dust in the upper mesosphere. J. Atmos. Sol. Terr. Phys. 118, 151–160. https://doi.org/10.1016/j.jastp.2013.11.008. smoke and Ice in the Mesosphere.

Rapp, M., Latteck, R., Stober, G., Hoffmann, P., Singer, W., Zecha, M., 2011a. First three-dimensional observations of polar mesosphere winter echoes: resolving space-time ambiguity. J. Geophys. Res. 116, A11307. https://doi.org/10.1029/2011JA016858.

Rapp, M., Lübken, F.J., 2004. Polar mesosphere summer echoes (pmse): review of observations and current understanding. Atmos. Chem. Phys. 4, 2601–2633. https://doi.org/10.5194/acp-4-2601-2004. https://www.atmos-chem-phys.net/4/2601/2004/.

Rapp, M., Lübken, F.J., 2003. On the nature of pmse: electron diffusion in the vicinity of charged particles revisited. J. Geophys. Res.: Atmosphere 108. https://doi.org/10.1029/2002JD002857. https://agupubs.onlinelibrary.wiley.com/doi/abs/10.1029/2002JD002857.

Rapp, M., Strelnikova, I., 2009. Measurements of meteor smoke particles during the ecoma-2006 campaign: 1. particle detection by active photoionization. J. Atmos. Sol. Terr. Phys. 71, 477–485. https://doi.org/10.1016/j.jastp.2008.06.002. global Perspectives on the Aeronomy of the Summer Mesopause Region. http://www.sciencedirect.com/science/article/pii/S1364682608001521.

Rapp, M., Strelnikova, I., Latteck, R., Hoffmann, P., Hoppe, U.P., Häggström, I., Rietveld, M., 2008. Polar mesosphere summer echoes (PMSE) studied at Bragg wavelengths of 2.8 m, 67 cm, and 16 cm. J. Atmos. Sol. Terr. Phys. 70, 947–961. https://doi.org/10.1016/j.jastp.2007.11.005.

Rapp, M., Strelnikova, I., Li, Q., Engler, N., Teiser, G., 2012. Charged aerosol effects on the scattering of radar waves from the D-region. In: Lübken, F.J. (Ed.), Climate and Weather of the Sun-Earth System (CAWSES): Highlights from a Priority Program. Springer, Dordrecht, The Netherlands. https://doi.org/10.1007/978-94-007-4348-9.

Rapp, M., Strelnikova, I., Strelnikov, B., Friedrich, M., Gumbel, J., Hoppe, U.P., Blix, T., Havnes, O., Bracikowski, P., Lynch, K., Knappmiller, S., 2011b. Microphysical properties of mesospheric aerosols: an overview of in situ-results from the ECOMA-project. In: Abdu, M.A., Pancheva, D., Bhattacharyya, A. (Eds.), Aeronomy of the Earth's Atmosphere and Ionosphere. Springer Science+Business Media B. V., pp. 67–74. https://doi.org/10.1007/978-94-007-0326-1-4. IAGA Special Sopron Book Series.

Rapp, M., Strelnikova, I., Strelnikov, B., Latteck, R., Baumgarten, G., Li, Q., Megner, L., Gumbel, J., Friedrich, M., Hoppe, U., Robertson, S., 2009. First in situ measurement of the vertical distribution of ice volume in a mesospheric ice cloud during the ECOMA/MASS rocket-campaign. Ann. Geophys. 27, 755–766.

Rapp, M., Thomas, G.E., 2006. Modeling the microphysics of mesospheric ice particles: assessment of current capabilities and basic sensitivities. J. Atmos. Sol. Terr. Phys. 68, 715–744.

Robertson, S., Dickson, S., Horányi, M., Sternovsky, Z., Friedrich, M., Janches, D., Megner, L., Williams, B., 2014. Detection of meteoric smoke particles in the mesosphere by a rocket-borne mass spectrometer. J. Atmos. Sol. Terr. Phys. 118, 161–179. https://doi.org/10.1016/j.jastp.2013.07.007. smoke and Ice in the Mesosphere.

Rosinski, J., Snow, R.H., 1961. Secondary particulate matter from meteor vapors. J. Atmos. Sci. 18, 736–745.

Röttger, J., La Hoz, C., Kelley, M.C., Hoppe, U.P., Hall, C., 1988. The structure and dynamics of polar mesosphere summer echoes observed with the EISCAT 224 MHz radar. Geophys. Res. Lett. 15, 1353–1356. https://doi.org/10.1029/GL015i012p01353.

Røyrvik, O., Smith, L.G., 1984. Comparison of mesospheric VHF radar echoes and rocket probe electron concentration measurements. J. Geophys. Res. 89, 9014–9022. https://doi.org/10.1029/JA089iA10p09014.

Shukla, P.K., 2001. A survey of dusty plasma physics. Phys. Plasmas 8, 1791–1803. https://doi.org/10.1063/1.1343087.

Shukla, P.K., Mamun, A.A., 2001. Introduction to dusty plasma physics. https://doi.org/10.1201/9781420034103.

Singer, W., Latteck, R., Holdsworth, D., 2008. A new narrow beam Doppler radar at 3mhz for studies of the high-latitude middle atmosphere. Adv. Space Res. 41, 1488–1494. https://doi.org/10.1016/j.asr.2007.10.006. http://www.sciencedirect.com/science/article/pii/S0273117707010307.

Skjelvan, B.W., 1994. Evaluation of Measurements with a Rocket-Borne Electron Probe. Diploma thesis, University of Trondheim.

Staszak, T., Asmus, H., Strelnikov, B., Lübken, F.J., Giono, G., 2017. A new rocket-borne Meteor Smoke Particle (MSPD) for D-region ionosphere. In: 23nd ESA Symposium on European Rocket and Balloon Programmes and Related Research, p. 201.

Staszak, T., Brede, M., Strelnikov, B., 2015. Open source software openfoam as a new aerodynamical simulation tool for rocket-borne measurements. In: Proceedings of the 22th ESA Symposium on European Rocket and Balloon Programmes and Related Research, pp. 201–207.

Staszak, T., Strelnikov, B., Latteck, R., Renkwitz, T., Friedrich, M., Baumgarten, G., Lübken, F.J., 2020. Turbulence generated small-scale structures as PMWE formation mechanism: results from rocket campaign. J. Atmos. Sol. Terr. Phys. submitted, this issue.

Strelnikov, B., Lübken, F.J., Rapp, M., Krein, G., Henkel, H., Heckl, H.J., 2015. TURB3D: new rocket-borne multi-sensor system to study three-dimensional structures of mesospheric turbulence. In: Ouwehand, L. (Ed.), 22nd ESA Symposium on European Rocket and Balloon Programmes and Related Research, p. 101.

Strelnikov, B., Rapp, M., 2011. In situ measurements of small-scale structures in neutrals and charged aerosols. In: Abdu, M.A., Pancheva, D., Bhattacharyya, A. (Eds.), Aeronomy of the Earth's Atmosphere and Ionosphere. Springer Science+Business Media B. V., pp. 83–91. https://doi.org/10.1007/978-94-007-0326-1-6. IAGA Special Sopron Book Series.

Strelnikov, B., Rapp, M., Lübken, F., 2013. In-situ density measurements in the mesosphere/lower thermosphere region with the TOTAL and CONE instruments. In: An Introduction to Space Instrumentation, pp. 1–11. https://doi.org/10.5047/aisi.001.

Strelnikov, B., Rapp, M., Lübken, F.J., 2003. Wavelet analysis applied to neutral density fluctuations measured in situ in the middle atmosphere. ESA 16, 321–326. https://ui.adsabs.harvard.edu/abs/2003ESASP.530..321S/abstract.

Strelnikov, B., Rapp, M., Strelnikova, I., Engler, N., Latteck, R., 2009. Small-scale structures in neutrals and charged aerosol particles as observed during the ECOMA/MASS rocket campaign. Ann. Geophys. 27, 1449–1456.

Strelnikova, I., Baumgarten, G., Lübken, F.J., 2020. Advanced hodograph-based analysis technique to derive gravity-wave parameters from lidar observations. Atmospheric Measurement Techniques 13, 479–499. https://doi.org/10.5194/amt-13-479-2020. https://www.atmos-meas-tech.net/13/479/2020/.

Strelnikova, I., Rapp, M., 2013. Statistical characteristics of PMWE observations by the EISCAT VHF radar. Ann. Geophys. 31, 359–375. https://doi.org/10.5194/angeo-31-359-2013.

Strelnikova, I., Rapp, M., Strelnikov, B., Baumgarten, G., Brattli, A., Svenes, K., Hoppe, U. P., Friedrich, M., Gumbel, J., Williams, B., 2009a. Measurements of meteor smoke particles during the ECOMA-2006 campaign: 2. Results. J. Atmos. Sol. Terr. Phys. 71, 486–496. https://doi.org/10.1016/j.jastp.2008.07.011.

Strelnikova, I., Rapp, M., Strelnikov, B., Baumgarten, G., Brattli, A., Svenes, K., Hoppe, U. P., Friedrich, M., Gumbel, J., Williams, B., 2009b. Measurements of meteor smoke particles during the ECOMA-2006 campaign: 2. Results. J. Atmos. Sol. Terr. Phys. 71, 486–496. https://doi.org/10.1016/j.jastp.2008.07.011.

Stude, J., Aufmhoff, H., Rapp, M., Schlager, H., Arnold, F., Strelnikov, B., 2020. A novel rocket borne ion mass spectrometer with large mass range: instrument description

and ↓first flight results. Atmospheric Measurement Techniques. https://doi.org/10.5194/amt-2020-203 submitted for publication.

Turunen, E., Matveinen, H., Tolvanen, J., Ranta, H., 1996. Step Handbook of Ionospheric Models. Scientific Committee on Solar-Terrestrial Physics, Toronto, Canada.

Varney, R.H., Kelley, M.C., Nicolls, M.J., Heinselman, C.J., Collins, R.L., 2011. The electron density dependence of polar mesospheric summer echoes. J. Atmos. Sol. Terr. Phys. 73, 2153–2165. https://doi.org/10.1016/j.jastp.2010.07.020.

von Zahn, U., Thrane, E.V., Skatteboe, R., 1995. The ALOMAR facility: status and outlook. In: Blix, T.A. (Ed.), Proceedings of the 12th ESA Symposium on European Rocket and Balloon Programmes and Related Research, Lillehammer, Norway, pp. 379–385.

Woodman, R.F., Guillen, A., 1974. Radar observations of winds and turbulence in the stratosphere and mesosphere. J. Atmos. Sci. 31, 493–505. https://doi.org/10.1175/1520-0469(1974)031<0493:ROOWAT>2.0.CO;2.